51st AIAA Aerospace Sciences Meeting including the New Horizons Forum and Aerospace Exposition
07 - 10 January 2013, Grapevine (Dallas/Ft. Worth Region), Texas

AIAA 2013-0225

The Construction of Analytic Hypersonic Pitch Moment Coefficients Using a Curl Transformation

Michael J. Grant*

Purdue University, West Lafayette, IN, 47906

This study investigates the creation of analytic hypersonic pitch moment coefficients by converting the traditional Newtonian surface integration into a mathematically equivalent curl calculation. This manipulation enables analytic pitch moment coefficients to be derived for shapes of increasing complexity. The analytic solutions are obtained by converting the physical moment calculation across the unshadowed surface to an equivalent volumetric curl calculation of a mathematical vector field that is directed away from the center of gravity location. This capability is made possible by the analytic expression of the Newtonian moment calculation and is not available in present-day studies that rely on approximate panel methods. The results of this investigation enable the construction of analytic relations for new hypersonic configurations of interest, and this approach serves as the foundation to construct efficient hybrid exact-approximate solutions for more complex configurations. A state-of-the-art hypersonic design tool validates all of the analytic relations developed in this investigation. The rapid longitudinal analysis made possible by the analytic pitch moment relations enable packaging considerations and trim control surface deflections to be incorporated into conceptual design studies.

Nomenclature

APAS	Aerodynamic Preliminary Analysis System
CBAERO	Configuration Based Aerodynamics
CFD	Computational Fluid Dynamics
GTS	GNU Triangulated Surface Library

A	first-order coefficient of exponential potential
A_1	lower surface
A_2	upper surface
A_{xy}	projection of area onto x-y plane
A_{ref}	reference area, m^2
B	zero-order coefficient of exponential potential
C	integration constant
C_D	drag force coefficient
C_L	lift force coefficient
C_N	normal force coefficient
C_l	roll moment coefficient
C_m	pitch moment coefficient
C_n	yaw moment coefficient
C_p	pressure coefficient
C_x	potential coefficient of x only
C_{xz}	potential coefficient shared by x and z
C_y	potential coefficient of y only
C_{yz}	potential coefficient shared by y and z
d	base diameter of vehicle, m
h	height of vehicle, m
l	length of parabola of revolution, m
l_{ref}	reference length, m
p	local surface pressure, Pa
p_∞	freestream pressure, Pa
r_n	nose radius, m
V_∞	freestream velocity, m/s
$\mathbf{df}$	differential force, N
$\mathbf{F}$	vector field
$\hat{\mathbf{n}}$	unit normal, m
$\mathbf{r}$	position vector, m

*Assistant Professor, School of Aeronautics and Astronautics, AIAA Member.

α	angle of attack, rad	ρ	potential radius, m
γ_x	angle between $\hat{\mathbf{n}}_{\mathbf{out}}$ and x axis	ρ_∞	freestream density, kg/m^3
γ_y	angle between $\hat{\mathbf{n}}_{\mathbf{out}}$ and y axis	ϕ	potential function
γ_z	angle between $\hat{\mathbf{n}}_{\mathbf{out}}$ and z axis	ω	revolution angle, rad
δ	flap deflection angle, rad		
δ_c	cone half angle, rad		
θ	angle between freestream and local normal, rad		

I. Introduction

Traditionally, the hypersonic aerodynamics of vehicles are modeled during conceptual design using Newtonian flow theory.[1,2] This theory assumes that when a particle (traveling in rectilinear motion) strikes the surface of a body, all of the momentum normal to the surface would be lost and all momentum tangential to the surface would be conserved as shown in Figure 1. Consequently, the pressure exerted by the fluid on the surface of a body is assumed to be solely originating from this loss of momentum normal to the surface. Under these assumptions, the nondimensional pressure coefficient, C_p, at any point on the surface of a body can be obtained from the Newtonian sine-squared relation shown in Eq. (1). Furthermore, the pressure exerted by the fluid on any portion of the surface not directly exposed to the flow, denoted as the shadowed region of the body, is assumed to be equivalent to the freestream pressure in which the motion of the fluid does not influence the pressure in this region. Consequently, $C_p = 0$ throughout the shadowed region as shown in Fig. 2.

$$C_p = \frac{p - p_\infty}{\frac{1}{2}\rho_\infty V_\infty^2} = 2\sin^2\theta \tag{1}$$

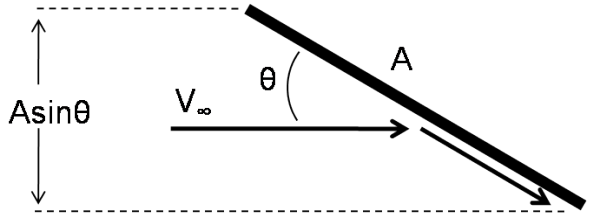

Figure 1: Momentum transfer of particle on inclined surface.[2]

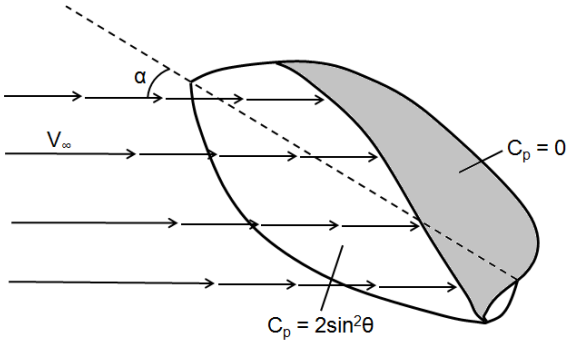

Figure 2: Example of shadowed body.[2]

The pressure that results from this momentum transfer is integrated over the unshadowed surface of the vehicle to calculate the hypersonic moment coefficients as shown in Eq. (2), where $\hat{\mathbf{n}}_{\mathbf{in}}$ is the inward unit normal and $\mathbf{df}$ is calculated from Eq. (3). In traditional conceptual design, this surface integration is approximated numerically in the form of panel methods such as those included within the Configuration Based Aerodynamics (CBAERO) tool[3] and the Aerodynamic Preliminary Analysis System (APAS).[4,5,6] Additionally, the aerodynamics of bodies of revolution have been calculated using ring approximation methods.[7,8,9] Although these conceptual numerical methods allow rapid aerodynamic calculations compared to computational fluid dynamics (CFD), this process must be repeated for any change in shape of the vehicle. Additionally, the resolution of the mesh must be addressed when using numerical methods. For example, the number of required panels to achieve a desired accuracy is generally unknown in the beginning of the meshing process. Consequently, multiple meshes of various resolutions must be evaluated until the convergence of aerodynamic coefficients is observed. The construction of a mesh for complicated shapes would also likely require modeling in a computer-aided design package. While certain tools such as CBAERO provide built-in routines to mesh bodies of revolution, other vehicle shapes must be meshed using external tools such as the GNU Triangulated Surface Library (GTS).[10] These time-consuming issues associated with panel methods

limit the number of vehicle shapes analyzed during conceptual design.

$$\begin{bmatrix} C_l \\ C_m \\ C_n \end{bmatrix} = \frac{1}{A_{ref}\ l_{ref}} \iint_S \begin{bmatrix} (\mathbf{r} \times \mathbf{df})^T \hat{\mathbf{x}} \\ (\mathbf{r} \times \mathbf{df})^T \hat{\mathbf{y}} \\ (\mathbf{r} \times \mathbf{df})^T \hat{\mathbf{z}} \end{bmatrix} = \frac{1}{A_{ref}\ l_{ref}} \iint_S \begin{bmatrix} (\mathbf{r} \times C_p\ \hat{\mathbf{n}}_{\mathbf{in}})^T \hat{\mathbf{x}} \\ (\mathbf{r} \times C_p\ \hat{\mathbf{n}}_{\mathbf{in}})^T \hat{\mathbf{y}} \\ (\mathbf{r} \times C_p\ \hat{\mathbf{n}}_{\mathbf{in}})^T \hat{\mathbf{z}} \end{bmatrix} \mathrm{d}A \tag{2}$$

$$\mathbf{df} = C_p\ \hat{\mathbf{n}}_{\mathbf{in}}\ \mathrm{d}A \tag{3}$$

I.A. Motivation for Analytic Hypersonic Aerodynamics

While panel methods would likely be required for the conceptual design of complicated geometries such as the Space Shuttle Orbiter, X-38, and HL-20, many hypersonic vehicle designs used in previous and current mission studies are not complex. For example, all previous and currently planned Mars missions have used blunt sphere-cones. Various human Mars mission studies have used blunt sphere-cones and blunted biconics.[11,12,13] The Stardust and Genesis Earth entries also used blunt sphere-cones.[14,15] The Apollo and Orion command modules both utilized a spherical forebody segment. Many high performance military hypersonic vehicles are slender sphere-cones and slender biconics with minor nose blunting to account for extreme heating environments. Some high performance entry vehicles include blended wedge designs, such as the SHARP L1, that consist of flat plates, conical frustums, and nose blunting through a cylindrical segment.[16] These examples represent a subset of missions that implement relatively simple vehicle geometries, and Figure 3 illustrates the wide range of applications for these vehicles.

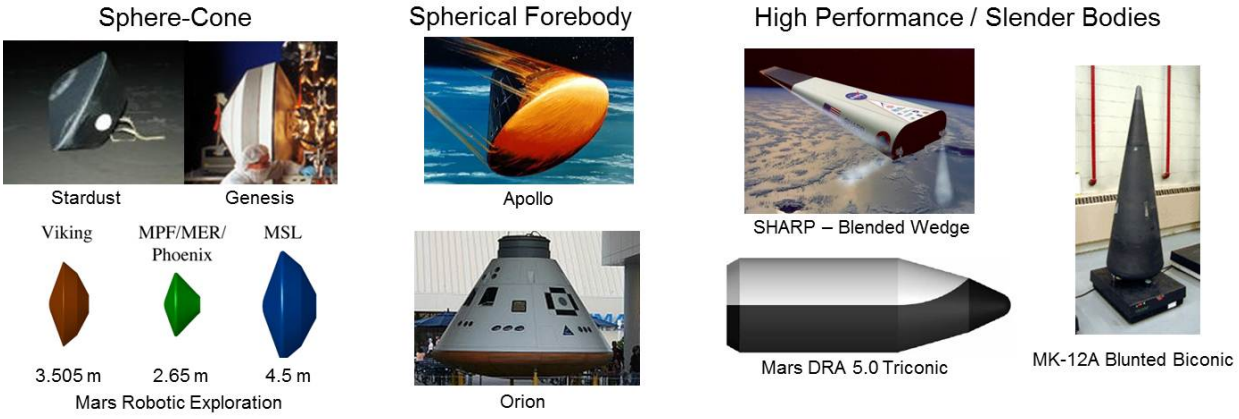

Figure 3: Example vehicles with analytic geometries.

The surface geometry of these basic shapes, along with additional complex shapes, can be expressed analytically. Consequently, the Newtonian surface integration that is traditionally performed numerically using panel methods can also be performed analytically. Many of the resulting analytic relations provide exact Newtonian aerodynamic coefficients currently approximated by panel methods. Additionally, the evaluation of most of the analytic relations is nearly instantaneous. As such, these relations could substitute panel methods widely used in traditional, segregated conceptual design environments to improve the computational performance of Newtonian aerodynamics calculations. More importantly, however, these relations eliminate the large aerodynamic tables that fundamentally segregate aerodynamics from other analyses during conceptual design and enable the construction of a unified, mathematical framework to perform rapid, simultaneous hypersonic aerodynamic and trajectory optimization.[17,18,19] The construction of analytic pitch moment coefficients enables this new, rapid design framework to be expanded to also include longitudinal analysis. For example, packaging considerations could be incorporated into this rapid design environment to identify valid trim angles of attack. For high-performance vehicles, the design and appropriate deflection of control surfaces (a procedure that is often neglected during conceptual design),[13,20,21] could also be incorporated into the rapid design environment. This enables the change in overall vehicle aerodynamics that results from various trim control surface deflections to be addressed during conceptual design. An example of each of these design benefits is provided at the end of this investigation.

I.B. Absence of Analytic Aerodynamics in Present-Day Analyses

The limited analytic relations developed in the 1950s and 1960s have largely been forgotten by the aerospace community in the recent decades. The manual development of analytic relations is time-intensive and requires complex integrations to be performed. As a result, the integration process is largely dependent on integral tables and appropriate substitutions, requiring substantial trial-and-error effort that is prohibitive during conceptual design. Rather, the advent of the digital computer resulted in the widespread adoption of panel and CFD methods over historical relations.[7,8,9,22,23,24,25,26] This can be observed by the many recent shape design studies that employ panel methods.[27,28]

Recent advances in symbolic manipulation tools, such as Mathematica[29] and Maple,[30] enable the modern construction of analytic relations for various shapes. These symbolic tools are capable of querying large databases of integral tables and substitution techniques, addressing some of the limitations that have historically prevented the adoption of analytic methods. Recent research has illustrated that the traditional Newtonian force calculation can be performed analytically for a wide range of basic shapes, including conical frustums, spherical segments, cylindrical segments, and flat plates, and this prior research complements the historical analytic relations.[31] Many common hypersonic vehicles of interest, including those shown in Figure 3, can be constructed through the superposition of these basic shapes. As such, the corresponding hypersonic force coefficients of each basic shape can also be combined to form analytic relations for vehicles of interest. However, as the complexity of the shape of the vehicle increases, the analytic solutions also increase in complexity. For certain complex shapes, no analytic force or moment solution can be constructed from the traditional Newtonian calculation. This is a consequence of the fundamental challenges that exist within the traditional calculations.

II. Fundamental Challenges of Traditional Newtonian Aerodynamics

The most apparent challenge during the integration process is that many simple functions cannot be analytically integrated. For example, the function $\sin(x)/x$ has no known analytic integral. As vehicles of greater complexity are considered, no guarantee can be made regarding the existence of a closed form, analytic solution. In recent analytic work,[31] simple bodies of revolution are analyzed as an attempt to expand the database to include more complex shapes. The surface of these bodies is naturally parametrized using trigonometric functions of the revolution angle. For an example spherical segment that could serve as the nose of a sphere-cone vehicle with cone half angle δ_c and nose radius r_n, the revolution angle, ω, shown in Figure 4 corresponds to the natural surface parametrization as described by Eq. (4). As a result, the corresponding shadow boundaries that determine the limits of the analytic integration are functions of inverse trigonometric functions. These functions, when combined with other polynomial expressions that appear during the integration process, generally result in expressions that cannot be analytically integrated. For certain combinations that are analytically integrable, the solutions obtained by symbolic manipulation tools such as Mathematica generally result in very lengthy expressions that reduce computational performance.

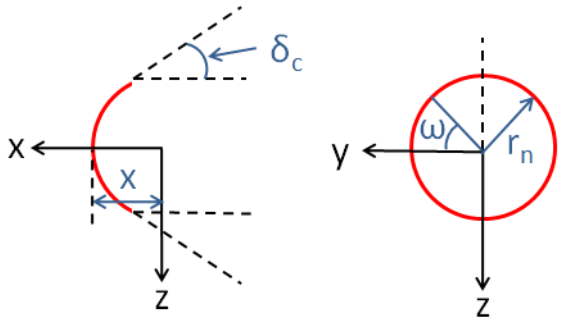

Figure 4: Side and front view of spherical segment parametrization.

$$\mathbf{r} = [x \quad \sqrt{r_n^2 - x^2}\cos(\omega) \quad -\sqrt{r_n^2 - x^2}\sin(\omega)]^T \tag{4}$$

To avoid the complexity of inverse trigonometric functions, bodies of revolution could be parametrized using Cartesian coordinates. While this parametrization eliminates the inverse trigonometric functions that appear in the shadow boundary, alternate inverse trigonometric functions appear from the mapping of Cartesian distances (used to provide integration limits that the describe the surface of the shape) to inverse trigonometric functions during integration. An example of a simple distance calculation that results in an inverse trigonometric function is shown in Eq. (5). A similar phenomenon also exists due to the normal vector normalizations required to calculate the pressure coefficient and direction of force used in Newtonian

moment calculations as shown in Eq. (3). As an example, the normalization term that appears in Eq. (6) also leads to an inverse trigonometric expression after integration. In fact, many vehicle configurations suffer from this inverse trigonometric complexity due to both of these complications.

$$\int \sqrt{1-x^2}\,\mathrm{d}x = \frac{1}{2}(x\sqrt{1-x^2} + \arcsin x) + C \tag{5}$$

$$\int \frac{1}{\sqrt{1-x^2}}\,\mathrm{d}x = \arcsin x + C \tag{6}$$

Prior work has shown that these challenges can be overcome in the construction of analytic force coefficients by converting the traditional Newtonian surface integration into a divergence calculation throughout the unshadowed volume of the vehicle.[32] In this approach, the traditional Newtonian surface integration is converted to an equivalent calculation of a mathematical flux that passes through the unshadowed surface of the vehicle. As an example, Eq. (7) illustrates that the normal force coefficient calculation can be converted into a flux calculation of a mathematical vector field with magnitude C_p that acts in a constant direction, $\hat{\mathbf{z}}$. This transformation enables the use of the Divergence Theorem, shown in Eq. (8), to convert the integration over the unshadowed surface, S, to a divergence calculation throughout the unshadowed volume, D.[33] This procedure removes the unit normal vector, $\hat{\mathbf{n}}_{\mathbf{out}}$, that originally existed in the traditional Newtonian surface integration. As a result, the integration process is favorably modified in manner that enables the construction of analytic force coefficients for vehicle configurations that are otherwise not possible when performing the traditional Newtonian surface integration.

$$\begin{aligned} C_N &= \frac{1}{A_{ref}} \iint_S C_p\ \hat{\mathbf{n}}_{\mathbf{in}}^T(-\hat{\mathbf{z}})\ \mathrm{d}A \\ &= \frac{1}{A_{ref}} \iint_S (C_p\ (-\hat{\mathbf{z}}))^T \hat{\mathbf{n}}_{\mathbf{in}}\ \mathrm{d}A \\ &= \frac{1}{A_{ref}} \iint_S (C_p\ \hat{\mathbf{z}})^T \hat{\mathbf{n}}_{\mathbf{out}}\ \mathrm{d}A \end{aligned} \tag{7}$$

$$\iint_S (C_p\ \hat{\mathbf{z}})^T \hat{\mathbf{n}}_{\mathbf{out}}\,\mathrm{d}A = \iiint_D \nabla^T (C_p\ \hat{\mathbf{z}})\,\mathrm{d}V \tag{8}$$

To construct analytic pitch moment coefficients for complex shapes, the unit normal vector in Eq. (2) must also be removed from the integration process. This is made possible by converting the traditional moment calculation into a mathematically equivalent curl calculation. The current analytic aerodynamic database, that includes the analytic relations derived in this investigation, can be downloaded from the following embedded file when viewed in Adobe Acrobat (aerodynamicsDatabase.zipREMOVEME)[a]. The enclosed Matlab routines should be referenced for the contents of the analytic expressions. When developing the analytic relations, each vehicle is parametrized such that the resulting solutions must only be developed once and are valid across all configurations. This is a major advantage over panel methods that must be executed each time the shape of the vehicle changes.

[a]Prior to unzipping the file, the 'REMOVEME' portion of the file extension must be removed.

III. Transformation of The Traditional Newtonian Moment Calculation

While the Divergence Theorem is often applied to flux calculations that result from the dot product[33] as shown in Eq. (8), a similar procedure can be used to derive an analogous form for the analytic moment calculations. The unit normal from Eq. (2) can be isolated as shown by Eq. (9) in which a mathematical vector field, $C_p\mathbf{r}$, is created. Note that this mathematical vector field acts along $\mathbf{r}$ that is defined relative to the c.g. and is independent of the direction of the freestream flow as shown in Fig. 5 for an example hemisphere with a c.g. located at the origin of the body axes. However, the magnitude of this mathematical vector field is a function of the pressure coefficient and, consequently, is a function of both vehicle shape and the relative orientation of the vehicle to the freestream flow. To eliminate the unit normal from the moment calculation, let γ_x, γ_y, and γ_z be the angles between $\hat{\mathbf{n}}_{\mathbf{out}}$ and the x, y, and z axes, respectively. As a result, $\hat{\mathbf{n}}_{\mathbf{out}} = [\cos\gamma_x, \cos\gamma_y, \cos\gamma_z]^T$, and the calculation from Eq. (9) can be expressed as shown in Eq. (10), where the mathematical vector field, $C_p\ \mathbf{r}$, is equivalent to $\mathbf{F} = [F_x, F_y, F_z]^T$ for brevity.

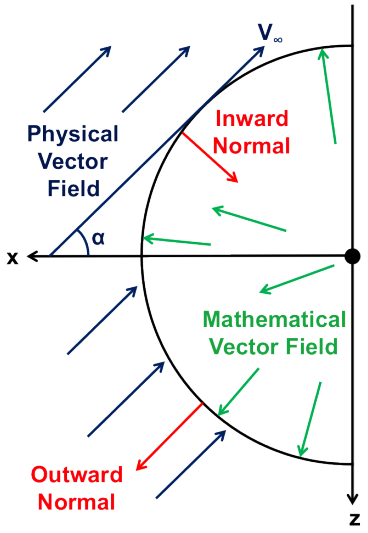

Figure 5: Comparison between physical and mathematical vector fields.

$$\begin{aligned}\frac{1}{A_{ref}\ l_{ref}} \iint_S \mathbf{r} \times C_p\ \hat{\mathbf{n}}_{\mathbf{in}}\ \mathrm{d}A &= \frac{1}{A_{ref}\ l_{ref}} \iint_S C_p\ \mathbf{r} \times \hat{\mathbf{n}}_{\mathbf{in}}\ \mathrm{d}A \\ &= \frac{1}{A_{ref}\ l_{ref}} \iint_S \hat{\mathbf{n}}_{\mathbf{out}} \times C_p\ \mathbf{r}\ \mathrm{d}A\end{aligned} \tag{9}$$

$$\frac{1}{A_{ref}\ l_{ref}} \iint_S \hat{\mathbf{n}}_{\mathbf{out}} \times \mathbf{F}\ \mathrm{d}A = \frac{1}{A_{ref}\ l_{ref}} \iint_S \begin{bmatrix} F_z\cos\gamma_y - F_y\cos\gamma_z \\ F_x\cos\gamma_z - F_z\cos\gamma_x \\ F_y\cos\gamma_x - F_x\cos\gamma_y \end{bmatrix} \mathrm{d}A \tag{10}$$

To remove $\hat{\mathbf{n}}_{\mathbf{out}}$ from the moment calculations, the surface integral shown in Eq. (10) can be elevated to a volume integral. An example of this elevation is shown in Eq. (11) for the first y-component term in Eq. (10). In this derivation, A_1 and A_2 serve as the lower and upper surfaces as shown in Fig. 6 for an example sphere, and A_{xy} serves as the projected area of the body onto the x-y plane where $\cos\gamma_z\ \mathrm{d}A = -dx\ dy$ on the lower surface. This procedure can be repeated across all permutations to eliminate the unit normal by elevating the surface integration to a volume integration as shown in Eq. (12). While this transformation would be of little use when numerically approximating the hypersonic moment coefficients due to the addition of a third integral, it enables the analytic moment calculation to be mapped to an analytic curl calculation of a vector field that is equivalent to $C_p\mathbf{r}$.

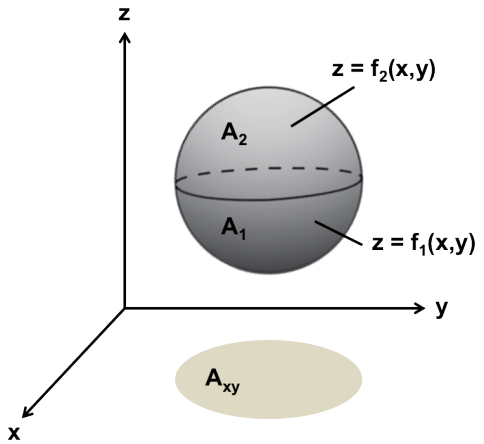

Figure 6: Example sphere regions for transformation from surface to volume integration.

$$
\begin{aligned}
\iint_S F_x \cos\gamma_z \, \mathrm{d}A &= \iint_{A_2} F_x \cos\gamma_z \, \mathrm{d}A + \iint_{A_1} F_x \cos\gamma_z \, \mathrm{d}A \\
&= \iint_{A_{xy}} F_x(x,y,f_2(x,y)) \, \mathrm{d}x \, \mathrm{d}y - \iint_{A_{xy}} F_x(x,y,f_1(x,y)) \, \mathrm{d}x \, \mathrm{d}y \\
&= \iint_{A_{xy}} \left[F_x(x,y,f_2(x,y)) - F_x(x,y,f_1(x,y)) \right] \mathrm{d}x \, \mathrm{d}y \\
&= \iint_{A_{xy}} \left[\int_{f_1(x,y)}^{f_2(x,y)} \frac{\partial F_x}{\partial z} \mathrm{d}z \right] \mathrm{d}x \, \mathrm{d}y \\
&= \iiint_V \frac{\partial F_x}{\partial z} \, \mathrm{d}x \, \mathrm{d}y \, \mathrm{d}z
\end{aligned}
\tag{11}
$$

$$
\begin{aligned}
\frac{1}{A_{ref} \; l_{ref}} \iint_S \hat{\mathbf{n}}_{\mathbf{out}} \times \mathbf{F} \, \mathrm{d}A &= \frac{1}{A_{ref} \; l_{ref}} \iiint_V \begin{bmatrix} \frac{\partial F_z}{\partial y} - \frac{\partial F_y}{\partial z} \\ \frac{\partial F_x}{\partial z} - \frac{\partial F_z}{\partial x} \\ \frac{\partial F_y}{\partial x} - \frac{\partial F_x}{\partial y} \end{bmatrix} \mathrm{d}V \\
&= \frac{1}{A_{ref} \; l_{ref}} \iiint_V \nabla \times \mathbf{F} \, \mathrm{d}V \\
&= \frac{1}{A_{ref} \; l_{ref}} \iiint_V \nabla \times C_p \mathbf{r} \, \mathrm{d}V
\end{aligned}
\tag{12}
$$

Since the traditional surface integration is only performed over the unshadowed surface of the vehicle, the analytic curl calculation must be performed throughout the unshadowed volume of the vehicle in a similar manner as described in prior work.[32] In this prior work, analytic force coefficients were constructed using an appropriate integration order across specified volumetric regions. Additionally, mathematical techniques were utilized to improve the analytic integration process. These techniques and considerations detailed in the prior work are also used in this investigation. Although this calculation has never been previously performed for Newtonian flow, the mapping between interior and boundary calculations provided by this analysis is similar to other aerodynamic applications that can be expressed using potential flow theory.[34]

IV. Application of the Analytic Curl Calculation to Various Shapes

To illustrate the advancements in analytic moment coefficients made possible by the analytic curl calculation, several select examples are provided. First, a series of quadratic shapes are analyzed to demonstrate that new analytic solutions can be obtained that are otherwise not possible when performing the traditional Newtonian moment calculation. Second, more complex semi-quadratic shapes are studied to illustrate the current limit in exact, analytic moment coefficients. Finally, solutions to parabolas of revolution are constructed to provide an example of computationally efficient, hybrid, exact-approximate solutions that are made possible by this approach. In the following examples, potential functions are used to describe each shape that is analyzed, Mathematica is used to perform the analytic integrations, and each solution is validated using CBAERO.

IV.A. Quadratic Potential Functions

Many high performance military hypersonic vehicles are slender sphere-cones and slender biconics with minor nose blunting to account for extreme heating environments. Spherical segments are often used to blunt the nose of these vehicles. As such, analytic moment coefficients are constructed for spherical segments that can be derived from the spherical potential shown in Eq. (13). To account for the wide range of possible c.g. locations for various hypersonic vehicles, the analytic moment coefficients are computed relative to any possible longitudinal c.g. location relative to the origin of the potential as shown in Fig. 7. Note that the portion of the spherical segment used to blunt sphere-cone and biconic vehicles is determined by the tangency conditions that must be enforced with the adjoining conical frustum with a cone half angle of δ_c. Currently, analytic moment relations have been found for a zero sideslip angle only. The analytic curl solutions for various spherical segments (δ_c = [5^o, 15^o, 30^o]) and c.g. locations (x_{cg} = [-2ρ, -6ρ, -10ρ] and z_{cg} = [2ρ, 4ρ, 5ρ]) are shown in Fig. 8, and these results are validated with the CBAERO solutions also shown. As expected, the roll and yaw moment coefficients are identically zero for this symmetric body at zero sideslip. The analytic stability derivatives, shown in Fig. 9, are also validated using a finite difference of the validated moment coefficients. Since conceptual hypersonic design studies frequently consist of bank and/or angle of attack control in which the vehicle travels with zero sideslip, only the analytic pitch moment coefficients are shown in the following results.

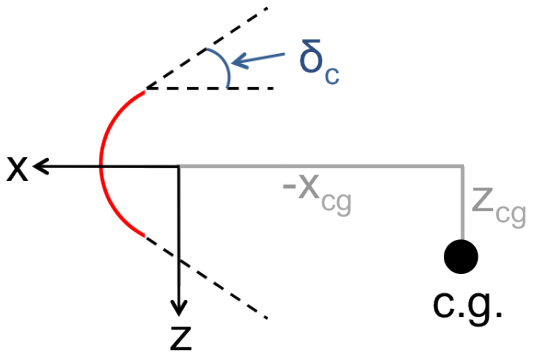

Figure 7: Spherical segment location relative to center of gravity.

$$\phi = x^2 + y^2 + z^2 = \rho^2 \tag{13}$$

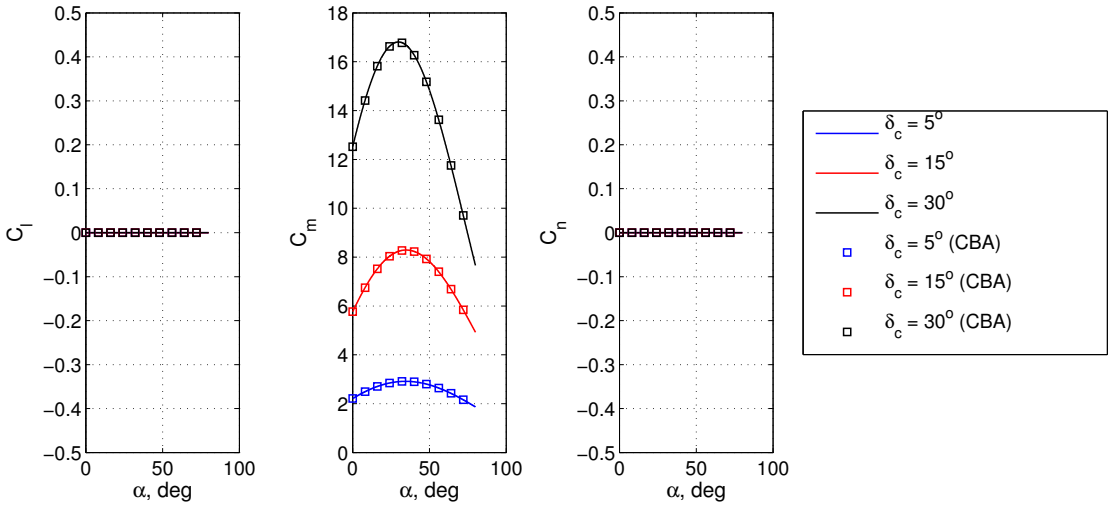

Figure 8: Spherical segment moment coefficient validation.

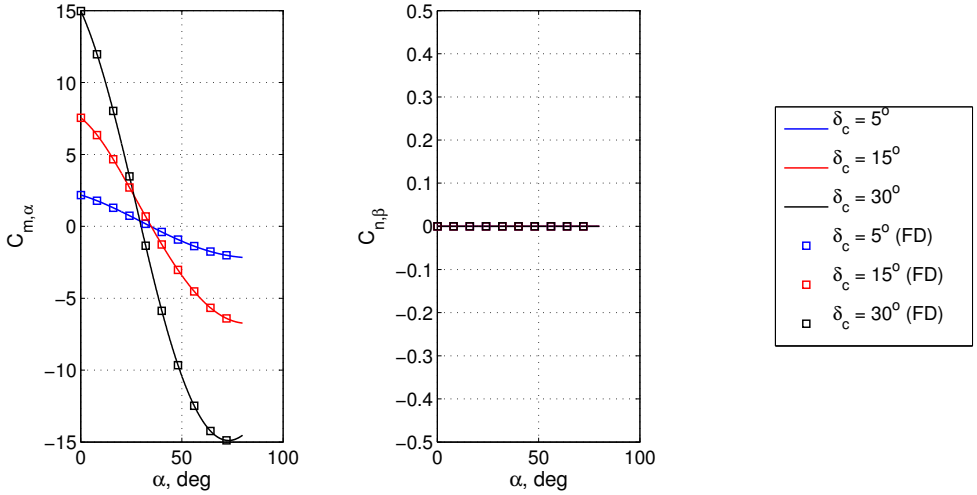

Figure 9: Spherical segment stability derivative validation.

To obtain analytic moments for more general forebody geometries to support conceptual hypersonic vehicle design, the complexity of the spherical potential is increased as shown in Eq. (14). This form enables the design of various axisymmetric nose segments as shown in Fig. 11. Note that this form enables a partial recovery of the potential function in the gradient magnitude that is only a function of one variable. For this potential, the recovery enables the gradient magnitude to be expressed only as a function of x as shown in Eq. (15). This property greatly reduces the complexities of the analytic integration process in manner similar to the benefits observed in prior work that investigated the construction of analytic force coefficients.[32] The pitch moment coefficients for the configurations shown in Fig. 11 and the same range of c.g. locations are validated using CBAERO as shown in Fig. 10 for $C_{yz} = \rho$.

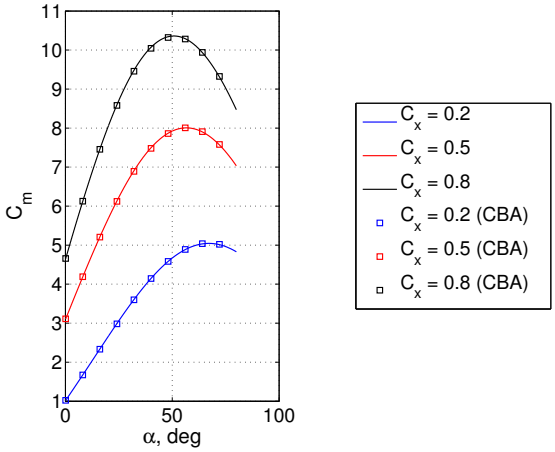

Figure 10: Quadratic potential validation for various C_x values.

$$\phi = C_x x^2 + C_{yz} y^2 + C_{yz} z^2 = \rho^2 \tag{14}$$

$$|\nabla \phi| = 2\sqrt{C_{yz}\rho^2 + C_x(C_x - C_{yz})x^2} \tag{15}$$

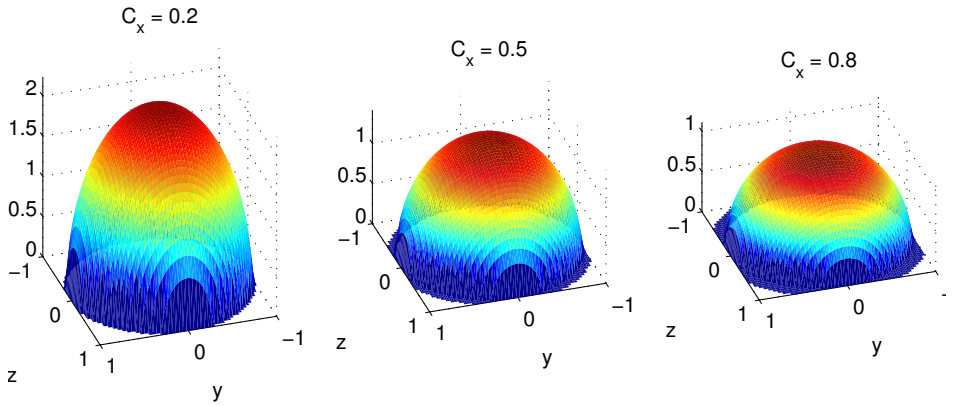

Figure 11: Validated shapes with various C_x values.

To enable the design of non-axisymmetric nose segments to support the conceptual design of high performance hypersonic systems, the complexity of the spherical potential is also increased as shown in Eq. (16). This geometry is effectively stretched in a manner that widens the nose for use on relatively flat and wide hypersonic systems such as Waveriders.[35,36] Note that this form also enables a partial recovery of the potential function in the gradient magnitude as shown in Eq. (17). The pitch moment coefficients for the configurations shown in Fig. 13 and the same range of c.g. locations are validated using CBAERO as shown in Fig. 12 for $C_{xz} = \rho$. Note that the analytic relations are only valid for $C_y < 1$, but this constraint is consistent with the geometry of practical hypersonic vehicles.

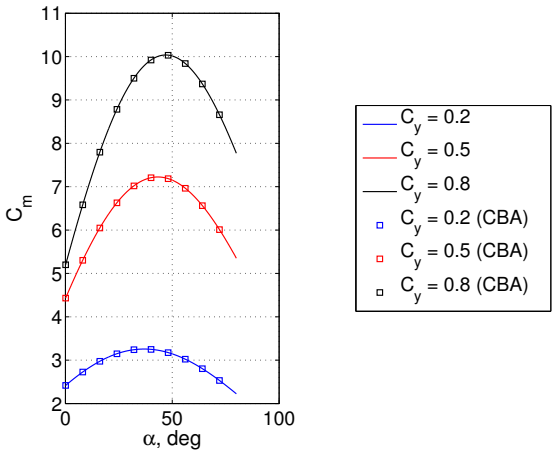

Figure 12: Quadratic potential validation for various C_y values.

$$\phi = C_{xz}x^2 + C_y y^2 + C_{xz}z^2 = \rho^2 \tag{16}$$

$$|\nabla\phi| = 2\sqrt{C_{xz}\rho^2 + C_y(-C_{xz} + C_y)y^2} \tag{17}$$

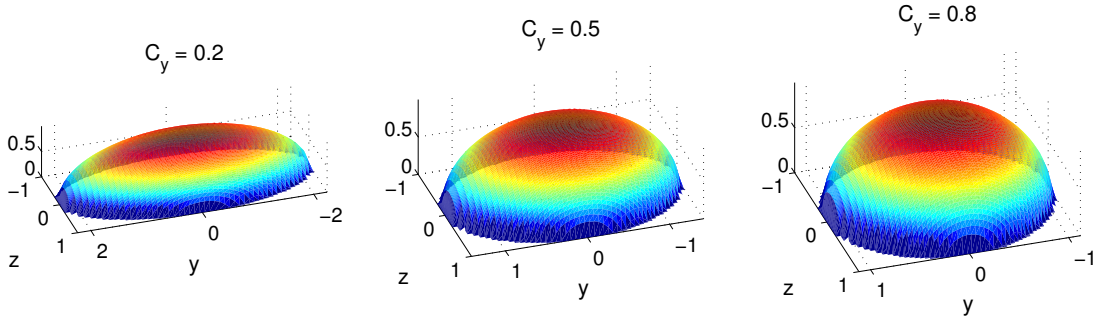

Figure 13: Validated shapes with various C_y values.

IV.B. Semi-Quadratic Potential Functions

The partial recovery of the potential function in the prior quadratic examples enables the construction of analytic moment coefficients using the curl formulation. For many of the potentials investigated beyond this quadratic form, no analytic solution could be found. As a result, a mathematical limit in the analytic moment relations appears to have been reached for this class of potentials. However, the potential function shown in Eq. (18) is an exception to this observation. The derivative property of this function results in a unique form in which the exponential terms can be combined using a complete-the-square technique. While the resulting analytic expressions in the database contain many individual imaginary terms, the combined result is purely real (to machine precision). The configurations shown in Figure 15 (where $B = 0$) for the same range of c.g. locations are validated using CBAERO as shown in Figure 14 where $C_{xz} = \rho$.

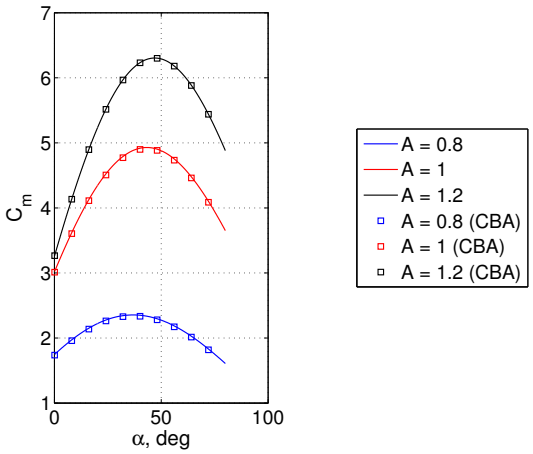

Figure 14: Quadratic exponential potential validation for various A values.

$$\phi = C_{xz}x^2 + e^{Ay+B} - e^B + C_{xz}z^2 = \rho^2 \tag{18}$$

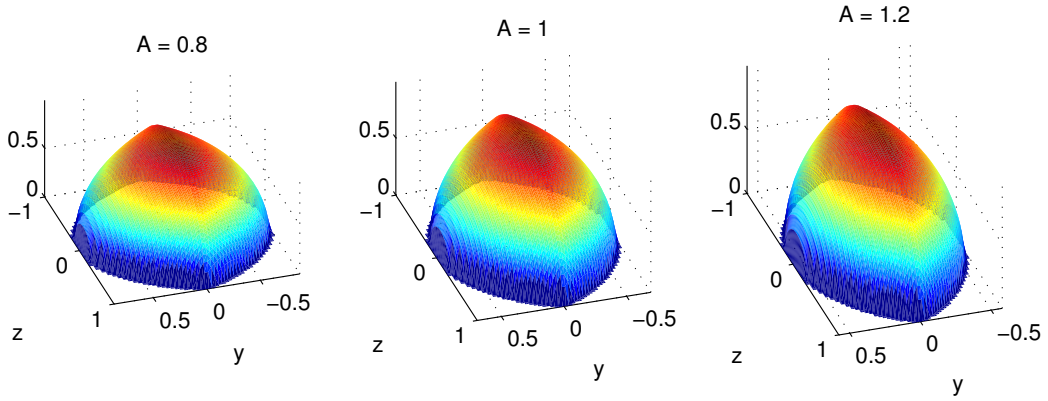

Figure 15: Validated shapes with various A values.

These results represent the current mathematical limit of exact pitch moment coefficients within the aerodynamic database. However, shapes outside of this exact database have solutions that can largely be represented with exact expressions and only require an approximation for a small portion of the solution. As such, the curl calculation serves as the cornerstone to develop hybrid exact-approximate moment coefficients. As each geometry is divided into various volumetric regions, an exact solution is found only if all integrations of each region can be performed analytically. For many shapes outside of the exact aerodynamic database, the majority of these regions can be integrated analytically and require no approximation. For the remaining regions, the first set of integrations can generally be performed analytically while the final integration must be approximated. If the expressions that must be approximated remain small relative to the exact expressions, then these hybrid exact-approximate analytic solutions would likely serve as a computationally efficient approximation. As an example, the pitch moment coefficient of a parabola of revolution can be constructed nearly exactly in which only a small set of expressions must be approximated.

IV.C. Parabola of Revolution

The parabola of revolution is described by the potential function shown in Eq. (19) with a gradient magnitude shown in Eq. (20). As illustrated, the potential recovery of the gradient is a function of x alone. For this class of shapes, only the final integration in x of two terms must be approximated for the pitch moment coefficient as shown in Eqs. (21) - (23), where the exact solution can also be found in the aerodynamic database. The limits of integration in x are determined by the corresponding volumetric region of which the integration is performed, where l is the length of the parabola of revolution.

$$\phi = x + y^2 + z^2 = 0 \tag{19}$$

$$|\nabla\phi| = \sqrt{1 - 4x} \tag{20}$$

$$C_m = C_m^{\text{exact}} + \frac{2}{A_{ref}\ l_{ref}} \int_{-l}^{-(1/4)\cot^2\alpha} (C_m^{\text{approx},1} + C_m^{\text{approx},2})\ \mathrm{d}x \tag{21}$$

$$C_m^{\text{approx},1} = \frac{2x \operatorname{arcsec}\left(\frac{2}{\sqrt{4+(\cot^2\alpha)/x}}\right)((-3+4x)z_{cg} - (3+4x)z_{cg}\cos 2\alpha + x(-7+12x-12x_{cg})\sin 2\alpha)}{3(1-4x)^2} \tag{22}$$

$$\begin{aligned} C_m^{\text{approx},2} =& (x \operatorname{arccsc}\left(\frac{2}{\sqrt{4+(\cot^2\alpha)/x}}\right)\csc\alpha(\cos 3\alpha(-3x_{cg} + 12xx_{cg} + (-x)^{3/2}\sqrt{-((4x+\cot^2\alpha)^2/x)}) \\ &+ \cos\alpha(-3(3+4x)x_{cg} + \sqrt{-x}x\sqrt{-((4x+\cot^2\alpha)^2/x)}) \\ &+ 4(-x)^{3/2}z_{cg}\sqrt{-((4x+\cot^2\alpha)^2/x)}\sin^3\alpha))/(3(1-4x)^2(4x+\cot^2\alpha)) \end{aligned} \tag{23}$$

Note that the above expressions that cannot be analytically integrated are approximated as a finite, analytic sum. As a result, the combined exact-approximate pitch moment coefficient is also fully analytic. This property enables vehicle geometries that have exact-approximate solutions to also be used within the rapid, simultaneous hypersonic aerodynamic and trajectory optimization framework described in Section I.A. Unlike panel methods, these expressions directly approximate the final aerodynamic result, and the error of this result can be directly controlled to obtain a desired accuracy. Alternatively, panel methods approximate vehicle shape to a certain level of accuracy, and the designer usually does not know *a priori* how this approximation translates to the accuracy of the aerodynamic coefficients. Consequently, multiple meshes of varying resolutions must be evaluated until convergence of the aerodynamic coefficients is observed. Using a trapezoidal approximation, the hybrid exact-approximate pitch moment coefficient for various parabolas of revolution shown in Figure 17 are validated for the same range of c.g. locations using CBAERO as shown in Figure 16.

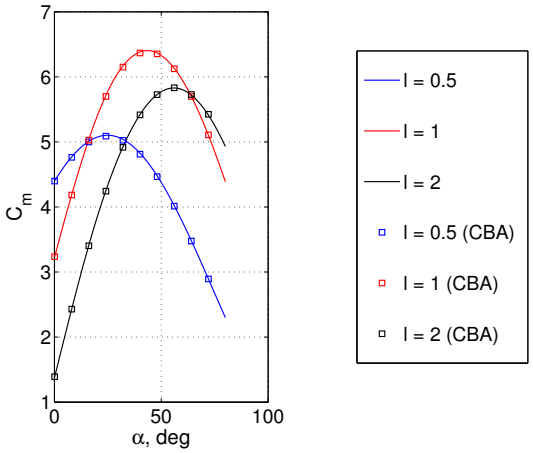

Figure 16: Parabola of revolution validation for various lengths.

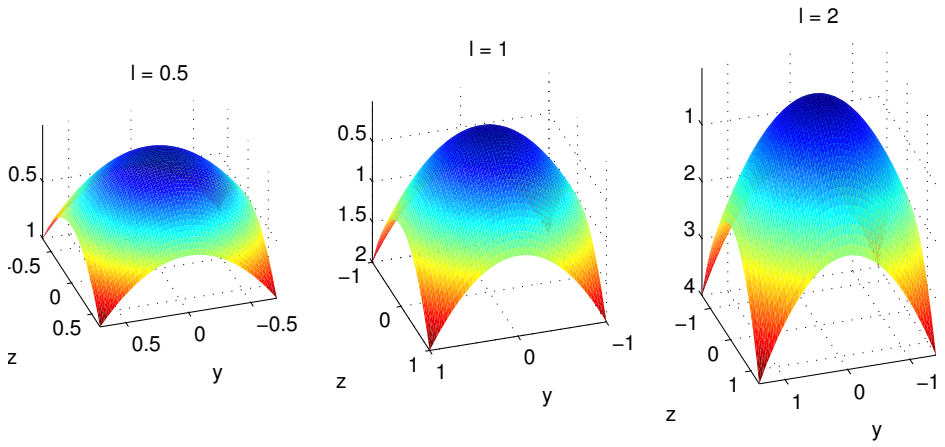

Figure 17: Validated shapes with various parabolic lengths.

V. Incorporation of Longitudinal Static Stability into Conceptual Design

The development and validation of analytic pitch moment coefficients enable the efficient incorporation of longitudinal static stability analysis into conceptual hypersonic design studies. The analytic relations provide a means to perform rapid analysis of trim c.g. locations and rapid design of control surfaces used to provide desired trim angles of attack. As shown in Fig. 3, many hypersonic applications utilize blunt sphere-cones and high-performance, slender biconics with geometries described in Figs. 19 and 20. These vehicles can be constructed by superimposing a spherical segment with an appropriate number of conical frustums of which analytic moment coefficients were derived in prior work.[31] As such, the aerodynamic moment coefficients of these individual components can also be combined to construct analytic moment coefficients of the entire vehicle. The combined pitch moment coefficients of both a sphere-cone and blunted biconic with parameters shown in Table 1 are validated using CBAERO as shown in Fig. 18.

Table 1: Sphere-cone and biconic parameters.

Parameter	*Sphere-Cone*	*Biconic*
r_n	0.3 ft.	1.0 in.
δ_1	70.0^o	17^o
δ_2	-	8^o
d	2.5 ft.	19.6 in.
h	-	48.0 in.
x_{cg}	0.2 ft.	10 in.
z_{cg}	0.1 ft.	4 in.

To illustrate the advantages of the analytic pitch moment coefficients, several design examples are provided. First, the trim c.g. locations of a blunt sphere-cone vehicle is identified. In this example, the analytic pitch moment coefficient enables the nearly instantaneous calculation of c.g. locations in which the coefficient vanishes. As illustrated in Fig. 18, the sphere-cone has a negative pitch moment slope, implying static stability for the c.g. locations found. Since the analytic relations are parametrized across all vehicle shape parameters and angles of attack, this procedure can be rapidly repeated for changes in geometry or flight orientations. As an example, the trim c.g. locations for the validated sphere-cone are shown in Figs. 21 and 22 for different angles of attack. As expected, the trim c.g. line is horizontal for small angles of attack and moves

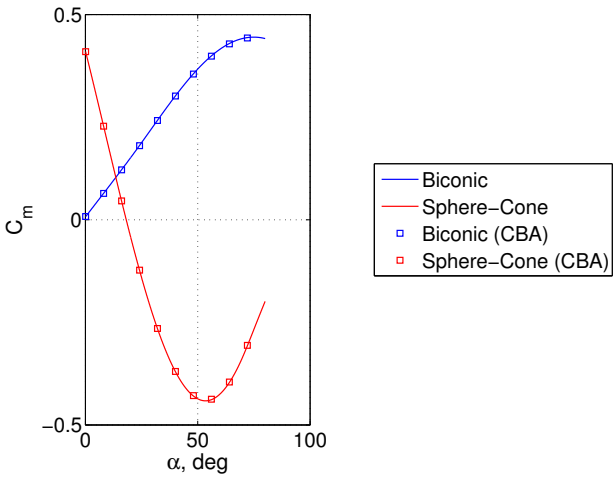

Figure 18: Biconic and sphere-cone validation.

downward as the angle of attack is increased. This type of analysis enables packaging considerations to determine valid angles of attack during flight. Additionally, the C_m magnitudes for various c.g. locations throughout the vehicle is also rapidly calculated, and the contours illustrate the reduction in magnitude with an increase in angle of attack. Analyses such as these could be used to quantify a measure of stability for incorporation into optimization studies.

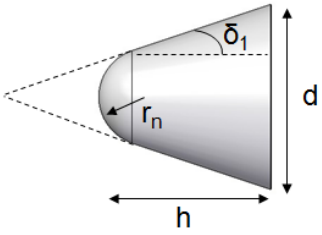

Figure 19: Sphere-cone parametrization.

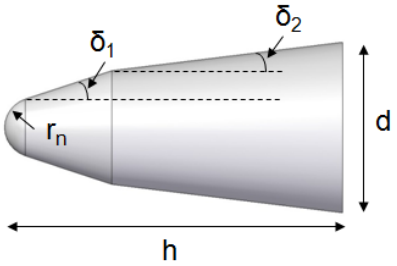

Figure 20: Biconic parametrization.

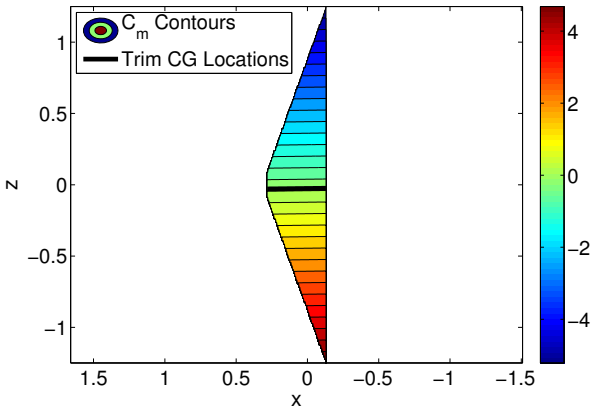

Figure 21: Longitudinal trim c.g. locations for $\alpha = 5^o$.

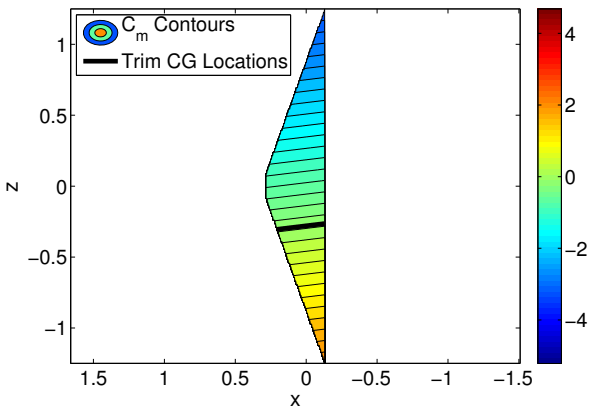

Figure 22: Longitudinal trim c.g. locations for $\alpha = 45^o$.

The analytic moment coefficients could also be used to incorporate control surface design into the overall hypersonic design process. Traditionally, conceptual design studies are executed using a table of aerodynamic coefficients obtained from a panel code such as CBAERO for various angles of attack. These tables are often incorporated into trajectory optimization routines that optimize the angle of attack profile to provide a desired flight path. In these early design studies, the mechanism by which the vehicle is capable of flying at various angles of attack is often neglected. In many applications, changes in angle of attack are accomplished through the deflection of a flap or other control surface. The deflection of control surfaces inherently alters the aerodynamic forces exerted on the vehicle, and as a consequence, alters the design of optimal trajectories. The analytic moment coefficients obtained in this investigation and the analytic force coefficients obtained in prior investigations[31,32] enable the rapid calculation of aerodynamic forces at various trim angles of attack. As an example, a body flap with a width of 15 in. and a height of 3 in. is attached to the bottom of the validated biconic as shown in Fig. 23, where the c.g. is chosen to be located $\frac{1}{4}h$ from the base along the axis of revolution. The trim flap deflection

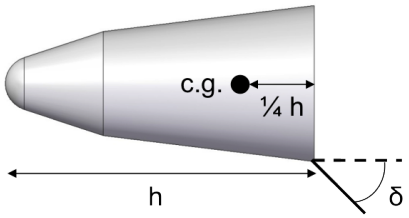

Figure 23: Example biconic with control surface.

angles, δ, are calculated for $5^o \leq \alpha \leq 25^o$ and are shown in Fig. 24. The corresponding change in the lift and drag coefficients is shown in Fig. 25. Note that the deflected flap increases both C_L and C_D substantially, and this illustrates the importance of incorporating static longitudinal stability analysis into trajectory design. The analytic relations enable real-time trim calculations to be performed during trajectory propagation, and as a result, provide a means to incorporate control surface design into conceptual hypersonic studies.

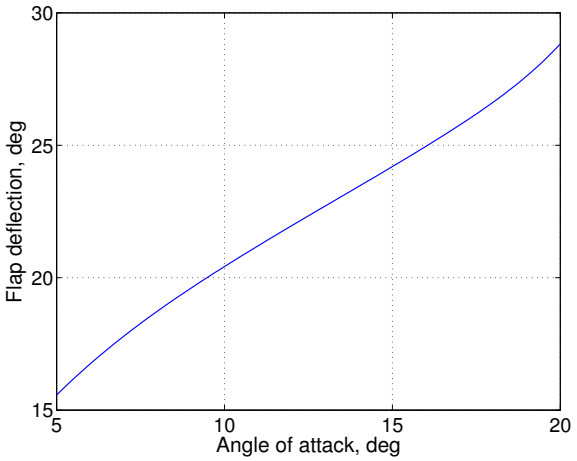

Figure 24: Flap deflection, δ, vs. angle of attack.

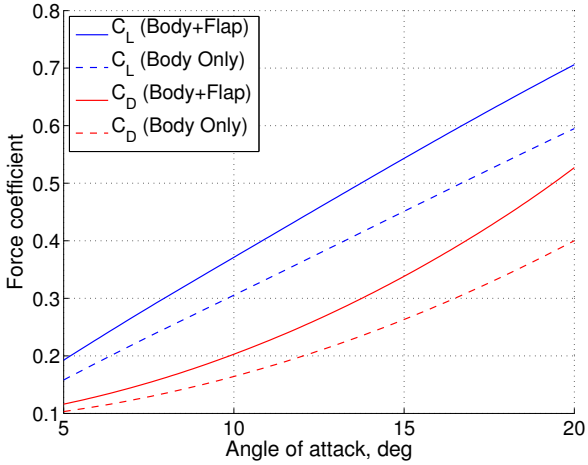

Figure 25: Change in aerodynamic coefficients due to trim flap deflections.

VI. Future Work

This work represents the current theoretical limit of the analytic moment coefficients using boundary-volume techniques. While the current analytic aerodynamic database can be leveraged to support the conceptual design of a wide range of hypersonic vehicles of interest, more generic analytic formulations would enable a wider range of geometries to be considered. As such, future research should focus on the development of analytic relations for a larger class of geometries. The development of a hybrid, exact-approximate analytic solution illustrates that approximation techniques could be used with the analytic curl calculation. The extent of hybrid solutions should be investigated as a potential means of greatly expanding the aerodynamic database. In this approach, the shape of the vehicle is specified, and the corresponding aerodynamics are calculated via integration. The challenges described in Section II often prevent the construction of analytic relations for many geometries, and these challenges may extend to the creation of hybrid, exact-approximate solutions. As such, the inverse aerodynamic problem should be studied in detail. In this approach, the analytic aerodynamics are specified *a priori*, and the shape of the vehicle could be approximated via differentiation of these analytic relations. Since differentiation is a relatively straightforward process, this approach would not be subject to the integration challenges observed in this investigation. As new solutions are developed, consideration must be given to methods that provide compact relations. The compact pitch moment coefficients developed in this investigation enable efficient incorporation into optimization techniques that rely on derivatives of the analytic relations, and the compact expressions greatly mitigate the increase in size and computational cost that results from the chain rule.

Additional considerations should also be made with regard to vehicle parametrization, integration limits, and integration order to capture new analytic solutions where possible. While the curl transformation discussed in this investigation has been largely automated, various mathematical techniques should be assembled in an automated manner to support the widespread search for analytic solutions. A computational framework is currently being developed on a high performance computing cluster at Purdue University to perform this search. Future computational frameworks should include an automated means of identifying partial analytic solutions to support the construction of hybrid, exact-approximate relations. As solutions to new configurations are explored, special consideration should be given to emerging technologies such as morphing or flexible structures. For example, analytic relations for inflatable aerodynamic decelerators would enable the real-time modeling of shape change during trajectory propagation. As such, these relations could

be used to improve the hypersonic modeling of passively flexible systems or to support targeting studies of actively controlled systems. Finally, analytic relations derived from fundamental models could also be obtained for non-Newtonian flow regimes such as free molecular flow to enable the rapid study of satellite orbital decay or trajectories of tumbling rocket bodies.[26]

VII. Summary

In this investigation, analytic hypersonic pitch moment coefficients are developed for both shadowed and unshadowed angles of attack based on Newtonian flow theory. To construct analytic solutions for new configurations of interest, the traditional Newtonian surface integration is transformed into a mathematically equivalent curl calculation throughout the unshadowed volume of the vehicle. While this conversion requires an additional integration to be performed, it also removes an existence of the unit normal from the integration process. As a result, the transformation avoids certain integration complexities and enables the construction of analytic solutions that are otherwise not possible. New analytic solutions are constructed for spherical segments often used for blunting of high performance hypersonic systems as well as additional quadratic geometries that enable new blunting configurations. These moment solutions, along with the analytic force solutions developed in prior work, represent the current limit in exact, analytic relations. For more complex configurations, a portion of the aerodynamics can be calculated exactly while the remaining terms require an approximation. The example parabola of revolution illustrates an efficient hybrid exact-approximate solution in which only two integrated terms must be approximated.

By combining the various geometries that currently exist within the analytic aerodynamic database, hypersonic vehicles of interest can be rapidly evaluated to support conceptual design and optimization studies. Two examples illustrate the nearly instantaneous analyses made possible by the analytic moment coefficients. The first example illustrates the rapid identification of trim c.g. locations within a sphere-cone for various angles of attack. This enables packaging considerations to be incorporated into the conceptual design process to identify reasonable trim angles of attack. The second example illustrates the rapid calculation of trim control surface deflections made possible by the analytic relations. This capability enables the change in vehicle aerodynamics to be rapidly calculated for deflections that provide the desired trim angle of attack. This capability advances the current state-of-the-art of conceptual hypersonic design studies that often do not incorporate the means by which vehicles achieve trim angles of attack. The analytic relations could substitute approximate panel methods widely used in traditional, segregated conceptual design environments. More importantly, however, these relations eliminate the large aerodynamic tables that fundamentally segregate aerodynamics from other analyses during conceptual design. As such, the relations developed in this investigation enable static longitudinal stability analysis to also be included within unified, mathematical design frameworks.

References

[1]Newton, I., *Principia - Motte's Translation Revised*, University of California Press, 1946.

[2]Anderson, J. D., *Hypersonic and High Temperature Gas Dynamics*, AIAA, 1989.

[3]Kinney, D. J., "Aero-Thermodynamics for Conceptual Design," AIAA-2004-31-962, *42nd AIAA Aerospace Sciences Meeting and Exhibit*, Reno, NV, 5-8 Jan. 2004.

[4]Bonner, E., Clever, W., and Dunn, K., "Aerodynamic Preliminary Analysis System II: Part I Theory," *NASA-CR-165627*, Apr. 1981.

[5]Smyth, D. N. and Loo, H. C., "Analysis of Static Pressure Data from 1/12-scale Model of the YF-12A. Volume 3: The MARK IVS Supersonic-Hypersonic Arbitrary Body Program, User's Manual," *NASA-CR-151940*, Oct. 1981.

[6]Cunningham, M., "Hypersonic Aerodynamics for an Entry Research Vehicle," *Journal of Spacecraft and Rockets*, Vol. 24, No. 2, 1987.

[7]Rainey, R. W., "Working Charts for Rapid Prediction of Force and Pressure Coefficients on Arbitrary Bodies of Revolution by Use of Newtonian Concepts," *NASA TN D-176*, 1959.

[8]Margolis, K., "Theoretical Evaluation of the Pressures, Forces, and Moments at Hypersonic Speeds Acting on Arbitrary Bodies of Revolution Undergoing Separate and Combined Angle-of-Attack and Pitching Motions," *NASA TN D-652*, 1961.

[9]Grimminger, G., Williams, E. P., and Young, G. B. W., "Lift on Inclined Bodies of Revolution in Hypersonic Flow," *Journal of the Aeronautical Sciences*, Vol. 17, No. 11, 1950.

[10]GTS Library Reference Manual, http://gts.sourceforge.net/reference/book1.html.

[11]Hoffman, S. J. and Kaplan, D. I., "Human Exploration of Mars: The Reference Mission of the NASA Mars Exploration Study Team," *NASA Special Publication 6107*, July 1997.

[12]Drake, B. G., "Reference Mission Version 3.0 Addendum to the Human Exploration of Mars: The Reference Mission of the NASA Mars Exploration Study Team," *NASA Special Publication 6107-ADD*, June 1998.

[13]Steinfeldt, B., Theisinger, J., Korzun, A., Clark, I., Grant, M., and Braun, R., "High Mass Mars Entry Descent and Landing Architecture Assessment," AIAA 2009-6684, *AIAA Space 2009*, Pasadena, CA, 14 - 17 Sept. 2009.

[14]Desai, P., Lyons, D., Tooley, J., and Kangas, J., "Entry, Descent, and Landing Operations Analysis for the Stardust Entry Capsule," *Journal of Spacecraft and Rockets*, Vol. 45, No. 6, 2008.

[15]Desai, P. and Lyons, D., "Entry, Descent, and Landing Operations Analysis for the Genesis Entry Capsule," *Journal of Spacecraft and Rockets*, Vol. 45, No. 1, 2008.

[16]Kinney, D. J. and Bowles, J. V., "Conceptual Design of a 'SHARP'-CTV," AIAA 2001-2887, *35th AIAA Thermophysics Conference*, Anaheim, CA, 11-14 Jun. 2001.

[17]Grant, M. J., Clark, I. G., and Braun, R. D., "Rapid Design Space Exploration for Conceptual Design of Hypersonic Missions," *AIAA Atmospheric Flight Mechanics Conference and Exhibit*, Portland, OR, 8-11 Aug. 2011.

[18]Grant, M. J., Clark, I. G., and Braun, R. D., "Rapid Simultaneous Hypersonic Aerodynamic and Trajectory Optimization Using Variational Methods," AIAA 2011-6640, *AIAA Atmospheric Flight Mechanics Conference and Exhibit*, Portland, OR, 8-11 Aug. 2011.

[19]Grant, M. J., *Rapid Simultaneous Hypersonic Aerodynamic and Trajectory Optimization for Conceptual Design*, PhD Thesis, Georgia Institute of Technology, School of Aerospace Engineering, May 2012.

[20]Garcia, J. A., Brown, J. L., Kinney, D. J., Bowles, J. V., Huynh, L. C., Jiang, X. J., Lau, E., and Dupzyk, I. C., "Co-Optimization of Mid Lift to Drag Vehicle Concepts for Mars Atmospheric Entry," AIAA 2010-5052, *10th AIAA/ASME Joint Thermophysics and Heat Transfer Conference*, Chicago, IL, 28 Jun. - 1 Jul. 2010.

[21]Armellin, R., Lavagna, M., Starkey, R. P., and Lewis, M. J., "Aerogravity-Assist Maneuvers: Coupled Trajectory and Vehicle Shape Optimization," *Journal of Spacecraft and Rockets*, Vol. 44, No. 5, 2007.

[22]Wells, W. and Armstrong, W., "Tables of Aerodynamic Coefficients Obtained From Developed Newtonian Expressions for Complete and Partial Conic and Spheric Bodies at Combined Angles of Attack and Sideslip with Some Comparisons with Hypersonic Experimental Data," *NASA TR R-127*, 1962.

[23]Eggers, A. J., Resnikoff, M. M., and Dennis, D. H., "Bodies of Revolution Having Minimum Drag at High Supersonic Airspeeds," *NACA TR-1306*, 1957.

[24]Elsgolc, L. D., *Calculus of Variations*, Dover Publications, Inc., 2007.

[25]Auman, L. M. and Wilks, B., "Supersonic and Hypersonic Minimum Drag for Bodies of Revolution," *AIAA 21st Applied Aerodynamics Conference*, Orlando, FL, 23-26 Jun. 2003.

[26]Regan, F. J. and Anandakrishnan, S. M., *Dynamics of Atmospheric Re-Entry*, AIAA, 1993.

[27]Theisinger, J. E. and Braun, R. D., "Multi-Objective Hypersonic Entry Aeroshell Shape Optimization," *Journal of Spacecraft and Rockets*, Vol. 46, No. 5, 2009.

[28]Kinney, D. J., "Aerodynamic Shape Optimization of Hypersonic Vehicles," AIAA 2006-239, *44th AIAA Aerospace Sciences Meeting and Exhibit*, Reno, NV, 9-12 Jan. 2006.

[29]Mathematica, Ver. 7, Wolfram Research, Champaign, IL.

[30]Maple, Ver. 13, Waterloo Maple Inc., Waterloo, Ontario, Canada.

[31]Grant, M. J. and Braun, R. D., "Analytic Hypersonic Aerodynamics for Conceptual Design of Entry Vehicles," AIAA 2010-1212, *48th AIAA Aerospace Sciences Meeting Including the New Horizons Forum and Aerospace Exposition*, Orlando, FL, 4-7 Jan. 2010.

[32]Grant, M. J. and Braun, R. D., "The Extension of Analytic Hypersonic Force Coefficients for Conceptual Design Using the Divergence Theorem," AIAA 2012-4580, *AIAA Atmospheric Flight Mechanics Conference and Exhibit*, Minneapolis, MN, 13-16 Aug. 2012.

[33]Thomas, G. B. and Finney, R. L., *Calculus*, Addison-Wesley Publishing Company, 1996.

[34]Anderson, J. D., *Fundamentals of Aerodynamics*, McGraw-Hill, 2001.

[35]Haney, J. W., "A Waverider Derived Hypersonic X-Vehicle," AIAA-95-6162, *AIAA Sixth International Aerospace Planes and Hypersonic Technologies Conference*, Chattanooga, TN, 3 - 7 Apr. 1995.

[36]Haney, J. W., Cervisi, R. T., Grantz, A. C., and Smith, T. R., "A Hypersonic Waverider Research Vehicle," AIAA-93-0402, *31st Aerospace Sciences Meeting and Exhibit*, Reno, NV, 11 - 14 Jan. 1993.